EUROPEAN ORGANIZATION FOR NUCLEAR RESEARCH

CERN–EP/2000-007
Revised Version

7 June 2000

Identified Charged Particles in Quark and Gluon Jets

DELPHI Collaboration

Abstract

A sample of 2.2 million hadronic Z decays, selected from the data recorded by the DELPHI detector at LEP during 1994-1995 was used for an improved measurement of inclusive distributions of π^+ , K^+ and p and their antiparticles in gluon and quark jets. The production spectra of the individual identified particles were found to be softer in gluon jets compared to quark jets, with a higher multiplicity in gluon jets as observed for inclusive charged particles. A significant proton enhancement in gluon jets is observed indicating that baryon production proceeds directly from colour objects. The maxima, ξ^*, of the ξ-distributions for kaons in gluon and quark jets are observed to be different.

(Eur. Phys. J. C17(2000)207)

P.Abreu[22], W.Adam[52], T.Adye[38], P.Adzic[12], Z.Albrecht[18], T.Alderweireld[2], G.D.Alekseev[17], R.Alemany[51], T.Allmendinger[18], P.P.Allport[23], S.Almehed[25], U.Amaldi[9,29], N.Amapane[47], S.Amato[49], E.G.Anassontzis[3], P.Andersson[46], A.Andreazza[9], S.Andringa[22], P.Antilogus[26], W-D.Apel[18], Y.Arnoud[9], B.Åsman[46], J-E.Augustin[26], A.Augustinus[9], P.Baillon[9], A.Ballestrero[47], P.Bambade[20], F.Barao[22], G.Barbiellini[48], R.Barbier[26], D.Y.Bardin[17], G.Barker[18], A.Baroncelli[40], M.Battaglia[16], M.Baubillier[24], K-H.Becks[54], M.Begalli[6], A.Behrmann[54], P.Beilliere[8], Yu.Belokopytov[9], K.Belous[44], N.C.Benekos[33], A.C.Benvenuti[5], C.Berat[15], M.Berggren[24], D.Bertrand[2], M.Besancon[41], M.Bigi[47], M.S.Bilenky[17], M-A.Bizouard[20], D.Bloch[10], H.M.Blom[32], M.Bonesini[29], M.Boonekamp[41], P.S.L.Booth[23], A.W.Borgland[4], G.Borisov[20], C.Bosio[43], O.Botner[50], E.Boudinov[32], B.Bouquet[20], C.Bourdarios[20], T.J.V.Bowcock[23], I.Boyko[17], I.Bozovic[12], M.Bozzo[14], M.Bracko[45], P.Branchini[40], R.A.Brenner[50], P.Bruckman[9], J-M.Brunet[8], L.Bugge[34], T.Buran[34], B.Buschbeck[52], P.Buschmann[54], S.Cabrera[51], M.Caccia[28], M.Calvi[29], T.Camporesi[9], V.Canale[39], F.Carena[9], L.Carroll[23], C.Caso[14], M.V.Castillo Gimenez[51], A.Cattai[9], F.R.Cavallo[5], V.Chabaud[9], M.Chapkin[44], Ph.Charpentier[9], P.Checchia[37], G.A.Chelkov[17], R.Chierici[47], P.Chliapnikov[9,44], P.Chochula[7], V.Chorowicz[26], J.Chudoba[31], K.Cieslik[19], P.Collins[9], R.Contri[14], E.Cortina[51], G.Cosme[20], F.Cossutti[9], H.B.Crawley[1], D.Crennell[38], S.Crepe[15], G.Crosetti[14], J.Cuevas Maestro[35], S.Czellar[16], M.Davenport[9], W.Da Silva[24], G.Della Ricca[48], P.Delpierre[27], N.Demaria[9], A.De Angelis[48], W.De Boer[18], C.De Clercq[2], B.De Lotto[48], A.De Min[37], L.De Paula[49], H.Dijkstra[9], L.Di Ciaccio[9,39], J.Dolbeau[8], K.Doroba[53], M.Dracos[10], J.Drees[54], M.Dris[33], A.Duperrin[26], J-D.Durand[9], G.Eigen[4], T.Ekelof[50], G.Ekspong[46], M.Ellert[50], M.Elsing[9], J-P.Engel[10], M.Espirito Santo[9], G.Fanourakis[12], D.Fassouliotis[12], J.Fayot[24], M.Feindt[18], A.Ferrer[51], E.Ferrer-Ribas[20], F.Ferro[14], S.Fichet[24], A.Firestone[1], U.Flagmeyer[54], H.Foeth[9], E.Fokitis[33], F.Fontanelli[14], B.Franek[38], A.G.Frodesen[4], R.Fruhwirth[52], F.Fulda-Quenzer[20], J.Fuster[51], A.Galloni[23], D.Gamba[47], S.Gamblin[20], M.Gandelman[49], C.Garcia[51], C.Gaspar[9], M.Gaspar[49], U.Gasparini[37], Ph.Gavillet[9], E.N.Gazis[33], D.Gele[10], T.Geralis[12], N.Ghodbane[26], I.Gil[51], F.Glege[54], R.Gokieli[9,53], B.Golob[9,45], G.Gomez-Ceballos[42], P.Goncalves[22], I.Gonzalez Caballero[42], G.Gopal[38], L.Gorn[1], Yu.Gouz[44], V.Gracco[14], J.Grahl[1], E.Graziani[40], P.Gris[41], G.Grosdidier[20], K.Grzelak[53], J.Guy[38], C.Haag[18], F.Hahn[9], S.Hahn[54], S.Haider[9], A.Hallgren[50], K.Hamacher[54], J.Hansen[34], F.J.Harris[36], F.Hauler[18], V.Hedberg[9,25], S.Heising[18], J.J.Hernandez[51], P.Herquet[2], H.Herr[9], T.L.Hessing[36], J.-M.Heuser[54], E.Higon[51], S-O.Holmgren[46], P.J.Holt[36], S.Hoorelbeke[2], M.Houlden[23], J.Hrubec[52], M.Huber[18], K.Huet[2], G.J.Hughes[23], K.Hultqvist[9,46], J.N.Jackson[23], R.Jacobsson[9], P.Jalocha[19], R.Janik[7], Ch.Jarlskog[25], G.Jarlskog[25], P.Jarry[41], B.Jean-Marie[20], D.Jeans[36], E.K.Johansson[46], P.Jonsson[26], C.Joram[9], P.Juillot[10], L.Jungermann[18], F.Kapusta[24], K.Karafasoulis[12], S.Katsanevas[26], E.C.Katsoufis[33], R.Keranen[18], G.Kernel[45], B.P.Kersevan[45], Yu.Khokhlov[44], B.A.Khomenko[17], N.N.Khovanski[17], A.Kiiskinen[16], B.King[23], A.Kinvig[23], N.J.Kjaer[9], O.Klapp[54], H.Klein[9], P.Kluit[32], P.Kokkinias[12], V.Kostioukhine[44], C.Kourkoumelis[3], O.Kouznetsov[17], M.Krammer[52], E.Kriznic[45], Z.Krumstein[17], P.Kubinec[7], J.Kurowska[53], K.Kurvinen[16], J.W.Lamsa[1], D.W.Lane[1], P.Langefeld[54], V.Lapin[44], J-P.Laugier[41], R.Lauhakangas[16], G.Leder[52], F.Ledroit[15], V.Lefebure[2], L.Leinonen[46], A.Leisos[12], R.Leitner[31], G.Lenzen[54], V.Lepeltier[20], T.Lesiak[19], M.Lethuillier[41], J.Libby[36], W.Liebig[54], D.Liko[9], A.Lipniacka[9,46], I.Lippi[37], B.Loerstad[25], J.G.Loken[36], J.H.Lopes[49], J.M.Lopez[42], R.Lopez-Fernandez[15], D.Loukas[12], P.Lutz[41], L.Lyons[36], J.MacNaughton[52], J.R.Mahon[6], A.Maio[22], A.Malek[54], T.G.M.Malmgren[46], S.Maltezos[33], V.Malychev[17], F.Mandl[52], J.Marco[42], R.Marco[42], B.Marechal[49], M.Margoni[37], J-C.Marin[9], C.Mariotti[9], A.Markou[12], C.Martinez-Rivero[20], F.Martinez-Vidal[51], S.Marti i Garcia[9], J.Masik[13], N.Mastroyiannopoulos[12], F.Matorras[42], C.Matteuzzi[29], G.Matthiae[39], F.Mazzucato[37], M.Mazzucato[37], M.Mc Cubbin[23], R.Mc Kay[1], R.Mc Nulty[23], G.Mc Pherson[23], C.Meroni[28], W.T.Meyer[1], E.Migliore[9], L.Mirabito[26], W.A.Mitaroff[52], U.Mjoernmark[25], T.Moa[46], M.Moch[18], R.Moeller[30], K.Moenig[9,11], M.R.Monge[14], D.Moraes[49], X.Moreau[24], P.Morettini[14], G.Morton[36], U.Mueller[54], K.Muenich[54], M.Mulders[32], C.Mulet-Marquis[15], R.Muresan[25], W.J.Murray[38], B.Muryn[19], G.Myatt[36], T.Myklebust[34], F.Naraghi[15], M.Nassiakou[12], F.L.Navarria[5], S.Navas[51], K.Nawrocki[53], P.Negri[29], N.Neufeld[9], R.Nicolaidou[41], B.S.Nielsen[30], P.Niezurawski[53], M.Nikolenko[10,17], V.Nomokonov[16], A.Nygren[25], V.Obraztsov[44], A.G.Olshevski[17], A.Onofre[22], R.Orava[16], G.Orazi[10], K.Osterberg[16], A.Ouraou[41], M.Paganoni[29], S.Paiano[5], R.Pain[24], R.Paiva[22], J.Palacios[36], H.Palka[19], Th.D.Papadopoulou[9,33], L.Pape[9], C.Parkes[9], F.Parodi[14], U.Parzefall[23], A.Passeri[40], O.Passon[54], T.Pavel[25], M.Pegoraro[37], L.Peralta[22], M.Pernicka[52], A.Perrotta[5], C.Petridou[48], A.Petrolini[14], H.T.Phillips[38], F.Pierre[41], M.Pimenta[22], E.Piotto[28], T.Podobnik[45], M.E.Pol[6], G.Polok[19], P.Poropat[48], V.Pozdniakov[17], P.Privitera[39], N.Pukhaeva[17], A.Pullia[29], D.Radojicic[36], S.Ragazzi[29], H.Rahmani[33], J.Rames[13], P.N.Ratoff[21], A.L.Read[34], P.Rebecchi[9], N.G.Redaelli[29], M.Regler[52], J.Rehn[18], D.Reid[32], R.Reinhardt[54], P.B.Renton[36], L.K.Resvanis[3], F.Richard[20], J.Ridky[13], G.Rinaudo[47], I.Ripp-Baudot[10], O.Rohne[34], A.Romero[47], P.Ronchese[37], E.I.Rosenberg[1], P.Rosinsky[7], P.Roudeau[20], T.Rovelli[5], Ch.Royon[41], V.Ruhlmann-Kleider[41], A.Ruiz[42], H.Saarikko[16], Y.Sacquin[41], A.Sadovsky[17], G.Sajot[15], J.Salt[51], D.Sampsonidis[12], M.Sannino[14], Ph.Schwemling[24], B.Schwering[54], U.Schwickerath[18], F.Scuri[48], P.Seager[21], Y.Sedykh[17], F.Seemann[54], A.M.Segar[36], N.Seibert[18], R.Sekulin[38], R.C.Shellard[6], M.Siebel[54], L.Simard[41], F.Simonetto[37], A.N.Sisakian[17], G.Smadja[26], O.Smirnova[25], G.R.Smith[38], A.Solovianov[44], A.Sopczak[18], R.Sosnowski[53], T.Spassov[22], E.Spiriti[40], S.Squarcia[14], C.Stanescu[40], S.Stanic[45], M.Stanitzki[18], K.Stevenson[36], A.Stocchi[20], J.Strauss[52], R.Strub[10], B.Stugu[4], M.Szczekowski[53], M.Szeptycka[53], T.Tabarelli[29], A.Taffard[23], O.Tchikilev[44], F.Tegenfeldt[50], F.Terranova[29], J.Thomas[36], J.Timmermans[32], N.Tinti[5], L.G.Tkatchev[17], M.Tobin[23], S.Todorova[9], A.Tomaradze[2], B.Tome[22], A.Tonazzo[9], L.Tortora[40], P.Tortosa[51], G.Transtromer[25], D.Treille[9], G.Tristram[8], M.Trochimczuk[53], C.Troncon[28], M-L.Turluer[41], I.A.Tyapkin[17], P.Tyapkin[25],

S.Tzamarias[12], O.Ullaland[9], V.Uvarov[44], G.Valenti[9,5], E.Vallazza[48], P.Van Dam[32], W.Van den Boeck[2], J.Van Eldik[9,32], A.Van Lysebetten[2], N.van Remortel[2], I.Van Vulpen[32], G.Vegni[28], L.Ventura[37], W.Venus[38,9], F.Verbeure[2], P.Verdier[26], M.Verlato[37], L.S.Vertogradov[17], V.Verzi[28], D.Vilanova[41], L.Vitale[48], E.Vlasov[44], A.S.Vodopyanov[17], G.Voulgaris[3], V.Vrba[13], H.Wahlen[54], C.Walck[46], A.J.Washbrook[23], C.Weiser[9], D.Wicke[54], J.H.Wickens[2], G.R.Wilkinson[36], M.Winter[10], M.Witek[19], G.Wolf[9], J.Yi[1], O.Yushchenko[44], A.Zalewska[19], P.Zalewski[53], D.Zavrtanik[45], E.Zevgolatakos[12], N.I.Zimin[17,25], A.Zintchenko[17], Ph.Zoller[10], G.C.Zucchelli[46], G.Zumerle[37]

[1]Department of Physics and Astronomy, Iowa State University, Ames IA 50011-3160, USA
[2]Physics Department, Univ. Instelling Antwerpen, Universiteitsplein 1, B-2610 Antwerpen, Belgium
and IIHE, ULB-VUB, Pleinlaan 2, B-1050 Brussels, Belgium
and Faculté des Sciences, Univ. de l'Etat Mons, Av. Maistriau 19, B-7000 Mons, Belgium
[3]Physics Laboratory, University of Athens, Solonos Str. 104, GR-10680 Athens, Greece
[4]Department of Physics, University of Bergen, Allégaten 55, NO-5007 Bergen, Norway
[5]Dipartimento di Fisica, Università di Bologna and INFN, Via Irnerio 46, IT-40126 Bologna, Italy
[6]Centro Brasileiro de Pesquisas Físicas, rua Xavier Sigaud 150, BR-22290 Rio de Janeiro, Brazil
and Depto. de Física, Pont. Univ. Católica, C.P. 38071 BR-22453 Rio de Janeiro, Brazil
and Inst. de Física, Univ. Estadual do Rio de Janeiro, rua São Francisco Xavier 524, Rio de Janeiro, Brazil
[7]Comenius University, Faculty of Mathematics and Physics, Mlynska Dolina, SK-84215 Bratislava, Slovakia
[8]Collège de France, Lab. de Physique Corpusculaire, IN2P3-CNRS, FR-75231 Paris Cedex 05, France
[9]CERN, CH-1211 Geneva 23, Switzerland
[10]Institut de Recherches Subatomiques, IN2P3 - CNRS/ULP - BP20, FR-67037 Strasbourg Cedex, France
[11]Now at DESY-Zeuthen, Platanenallee 6, D-15735 Zeuthen, Germany
[12]Institute of Nuclear Physics, N.C.S.R. Demokritos, P.O. Box 60228, GR-15310 Athens, Greece
[13]FZU, Inst. of Phys. of the C.A.S. High Energy Physics Division, Na Slovance 2, CZ-180 40, Praha 8, Czech Republic
[14]Dipartimento di Fisica, Università di Genova and INFN, Via Dodecaneso 33, IT-16146 Genova, Italy
[15]Institut des Sciences Nucléaires, IN2P3-CNRS, Université de Grenoble 1, FR-38026 Grenoble Cedex, France
[16]Helsinki Institute of Physics, HIP, P.O. Box 9, FI-00014 Helsinki, Finland
[17]Joint Institute for Nuclear Research, Dubna, Head Post Office, P.O. Box 79, RU-101 000 Moscow, Russian Federation
[18]Institut für Experimentelle Kernphysik, Universität Karlsruhe, Postfach 6980, DE-76128 Karlsruhe, Germany
[19]Institute of Nuclear Physics and University of Mining and Metalurgy, Ul. Kawiory 26a, PL-30055 Krakow, Poland
[20]Université de Paris-Sud, Lab. de l'Accélérateur Linéaire, IN2P3-CNRS, Bât. 200, FR-91405 Orsay Cedex, France
[21]School of Physics and Chemistry, University of Lancaster, Lancaster LA1 4YB, UK
[22]LIP, IST, FCUL - Av. Elias Garcia, 14-1^{o}, PT-1000 Lisboa Codex, Portugal
[23]Department of Physics, University of Liverpool, P.O. Box 147, Liverpool L69 3BX, UK
[24]LPNHE, IN2P3-CNRS, Univ. Paris VI et VII, Tour 33 (RdC), 4 place Jussieu, FR-75252 Paris Cedex 05, France
[25]Department of Physics, University of Lund, Sölvegatan 14, SE-223 63 Lund, Sweden
[26]Université Claude Bernard de Lyon, IPNL, IN2P3-CNRS, FR-69622 Villeurbanne Cedex, France
[27]Univ. d'Aix - Marseille II - CPP, IN2P3-CNRS, FR-13288 Marseille Cedex 09, France
[28]Dipartimento di Fisica, Università di Milano and INFN-MILANO, Via Celoria 16, IT-20133 Milan, Italy
[29]Dipartimento di Fisica, Univ. di Milano-Bicocca and INFN-MILANO, Piazza delle Scienze 2, IT-20126 Milan, Italy
[30]Niels Bohr Institute, Blegdamsvej 17, DK-2100 Copenhagen Ø, Denmark
[31]IPNP of MFF, Charles Univ., Areal MFF, V Holesovickach 2, CZ-180 00, Praha 8, Czech Republic
[32]NIKHEF, Postbus 41882, NL-1009 DB Amsterdam, The Netherlands
[33]National Technical University, Physics Department, Zografou Campus, GR-15773 Athens, Greece
[34]Physics Department, University of Oslo, Blindern, NO-1000 Oslo 3, Norway
[35]Dpto. Fisica, Univ. Oviedo, Avda. Calvo Sotelo s/n, ES-33007 Oviedo, Spain
[36]Department of Physics, University of Oxford, Keble Road, Oxford OX1 3RH, UK
[37]Dipartimento di Fisica, Università di Padova and INFN, Via Marzolo 8, IT-35131 Padua, Italy
[38]Rutherford Appleton Laboratory, Chilton, Didcot OX11 OQX, UK
[39]Dipartimento di Fisica, Università di Roma II and INFN, Tor Vergata, IT-00173 Rome, Italy
[40]Dipartimento di Fisica, Università di Roma III and INFN, Via della Vasca Navale 84, IT-00146 Rome, Italy
[41]DAPNIA/Service de Physique des Particules, CEA-Saclay, FR-91191 Gif-sur-Yvette Cedex, France
[42]Instituto de Fisica de Cantabria (CSIC-UC), Avda. los Castros s/n, ES-39006 Santander, Spain
[43]Dipartimento di Fisica, Università degli Studi di Roma La Sapienza, Piazzale Aldo Moro 2, IT-00185 Rome, Italy
[44]Inst. for High Energy Physics, Serpukov P.O. Box 35, Protvino, (Moscow Region), Russian Federation
[45]J. Stefan Institute, Jamova 39, SI-1000 Ljubljana, Slovenia and Laboratory for Astroparticle Physics,
Nova Gorica Polytechnic, Kostanjeviska 16a, SI-5000 Nova Gorica, Slovenia,
and Department of Physics, University of Ljubljana, SI-1000 Ljubljana, Slovenia
[46]Fysikum, Stockholm University, Box 6730, SE-113 85 Stockholm, Sweden
[47]Dipartimento di Fisica Sperimentale, Università di Torino and INFN, Via P. Giuria 1, IT-10125 Turin, Italy
[48]Dipartimento di Fisica, Università di Trieste and INFN, Via A. Valerio 2, IT-34127 Trieste, Italy
and Istituto di Fisica, Università di Udine, IT-33100 Udine, Italy
[49]Univ. Federal do Rio de Janeiro, C.P. 68528 Cidade Univ., Ilha do Fundão BR-21945-970 Rio de Janeiro, Brazil
[50]Department of Radiation Sciences, University of Uppsala, P.O. Box 535, SE-751 21 Uppsala, Sweden
[51]IFIC, Valencia-CSIC, and D.F.A.M.N., U. de Valencia, Avda. Dr. Moliner 50, ES-46100 Burjassot (Valencia), Spain
[52]Institut für Hochenergiephysik, Österr. Akad. d. Wissensch., Nikolsdorfergasse 18, AT-1050 Vienna, Austria
[53]Inst. Nuclear Studies and University of Warsaw, Ul. Hoza 69, PL-00681 Warsaw, Poland
[54]Fachbereich Physik, University of Wuppertal, Postfach 100 127, DE-42097 Wuppertal, Germany

1 Introduction

The different colour charges of quarks and gluons lead to specific differences in the particle multiplicity, the energy spectrum and the angular distributions of the corresponding jets. Beyond the study of these differences [1], which are related to the perturbative properties of QCD[1] elementary fields, the comparison of gluon and quark jets opens up the possibility to infer properties of the non-perturbative formation of hadrons directly.

The study of ratios of identified ($\pi^{\pm}, K^{\pm}, p(\bar{p})$) particle distributions in gluon (g) and quark (q) jets is the main subject of this paper.

Gluon jets are selected in $b\bar{b}g$ events by tagging the b quarks using techniques based on the large impact parameters of tracks coming from heavy particle decays. The Ring Imaging Cherenkov Counters (RICH) of the DELPHI detector provide particle identification over a wide momentum range in combination with the ionization loss measurement of the Time Projection Chamber (TPC) and so allow a detailed comparison of identified particle spectra in gluon and quark jets. These are used for a detailed test of QCD based fragmentation models and also to check MLLA[2] and LPHD[3] predictions [2].

This paper is organized as follows. In Section 2 the hadronic event selection, the quark/gluon separation, and the particle identification are described briefly. The experimental results are presented and compared with the predictions of models in Section 3. Finally a summary and conclusions are presented in Section 4.

2 Experimental Technique and Event Sample

A description of the DELPHI detector, together with a description of its performance, can be found in [3].

2.1 Event Selections

The data collected by DELPHI during 1994-1995 are considered in the present analysis, during which time the RICH [3] detectors (the main particle identification detectors) were fully operational and the Vertex detector was equipped with a three-dimensional readout. The cuts applied to charged and neutral particles and to events in order to select hadronic Z decays are identical to those given in [4] and [5]. The data sample passing the selection of hadronic events contained 1,775,230 events with a small contamination ($< 0.7\%$) arising from $\tau^+\tau^-$ pairs, beam-gas scattering and $\gamma\gamma$ interactions [3].

The influence of the detector performance on the analysis was studied with the full DELPHI simulation program, DELSIM [3]. Events generated with the JETSET 7.3 Parton Shower (PS) model [6], with parameters tuned by DELPHI [7], were passed through DELSIM and processed with the same reconstruction and analysis programs as the real data.

Three-jet events were clustered using the Durham algorithm [8] with a jet resolution parameter $y_{cut} = 0.015$. The value used for the cut-off was optimized using the JETSET 7.3 PS model, by maximizing the statistics available and the quark/gluon purity attained for the three-jet event samples [9].

The jet axes were projected onto the event plane, defined as the plane perpendicular to the smallest sphericity eigenvector obtained from the quadratic momentum tensor,

[1] **Q**uantum**C**hromo**D**ynamics
[2] **M**odified **L**eading **L**og **A**pproximation
[3] **L**ocal **P**arton **H**adron **D**uality

$M_{\alpha\beta} = \sum_{i=1}^{n} p_{i\alpha} p_{i\beta}$. The jets were numbered in decreasing order of jet energy, where the energy of each jet is calculated from the angles between the jets assuming massless kinematics:

$$E_j^{calc} = \frac{\sin\theta_j}{\sin\theta_1 + \sin\theta_2 + \sin\theta_3}\sqrt{s}, \quad j = 1, 2, 3\,, \tag{1}$$

where θ_j is the interjet angle as defined in Figure 1.

For a detailed comparison of quark and gluon jet properties, it is necessary to obtain samples of quark and gluon jets with similar kinematics and the same underlying scales [10]. To fulfill this condition, two different event topologies were used, as illustrated in Figure 1:

- mirror symmetric events, with θ_2 and $\theta_3 \in [150° - 15°, 150° + 15°]$, subsequently called **Y events**, and
- three-fold symmetric events, with θ_2 and $\theta_3 \in [120° - 15°, 120° + 15°]$, subsequently called **Mercedes events**.

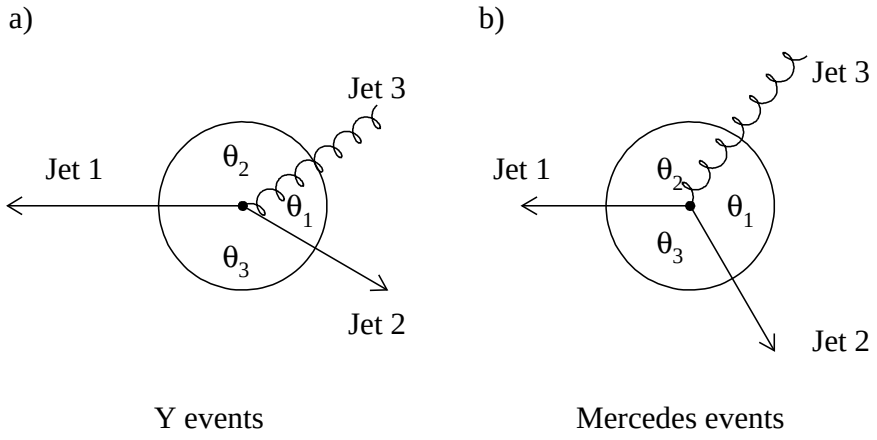

Figure 1: Event topologies of symmetric Y events and Mercedes events; θ_i are the angles between the jets after projection into the event plane.

For Y events only the low energy jets (jets 2 and 3 in Figure 1) were used in the analysis. For Mercedes events all jets were used in the analysis. The appropriate scale for these jets, equivalent to the e^+e^- beam energy can be approximated by $\kappa = E_{jet} \sin\theta_1/2$ [10]. Mercedes events are mainly used to study the scale dependence of particle production.

In order to enhance the contribution from events with three well-defined jets attributed to $q\bar{q}g$ production, further cuts (sum of angles between jet, polar angle of each jet axis, visible jet energy per jet and number of particles in each jet) are applied to the three-jet event samples, as in [4]. The number of three-jet events in the Mercedes and Y samples is 11,685 and 110,628 respectively.

2.2 Quark and Gluon Jet Identification

The identification of gluon jets by anti-tagging of heavy quark jets is identical to that described in [4]. Heavy quark tagging is based on large impact parameters with respect to the primary vertex due to the long lifetime of the heavy particles.

The efficiency and purity calculations were made using events generated by the JETSET 7.3 Monte Carlo model tuned to DELPHI data [7] and passed through DELSIM.

Even in simulated events, the assignment of parton flavours to the jets is not unique, as the decay history is interrupted by the building of strings in models such as JETSET or by the parton assignment of clusters in the case of HERWIG. Thus two independent ways of defining the gluon jet in the fully simulated events were investigated. The first method assumed that the jet which has the largest angle to hadrons containing heavy quarks is the gluon induced jet [4] (angle assignment) and in the second method the jet containing the fewest decay particles from the heavy hadrons was assigned to the gluon (history assignment). Both methods give similar results and therefore the purities can be estimated with small systematic uncertainties [5].

Gluon jet purities of $\sim 82\%$ for Y events and Mercedes events were achieved. Here the purity is defined as the ratio of correctly identified gluon jets to the total number of jets tagged as gluons. There are 24,449 events with an identified gluon jet in the case of Y events and 1,806 in the case of Mercedes events.

2.2.1 Corrections

Y	**quark content** (*dusc*)	*b* **quark content**	**gluon content**
normal mixture	49.5%	1.6%	48.9%
b tagged jets	25.1%	58.2%	16.6%
gluon tagged jets	13.7%	4.2%	82.0%
Mercedes	**quark content** (*dusc*)	*b* **quark content**	**gluon content**
normal mixture	64.2%	2.3%	33.3%
b tagged jets	17.3%	73.6%	9.1%
gluon tagged jets	11.1%	6.8%	81.8%

Table 1: Compositions of different jet classes in Y and Mercedes events. The statistical errors are smaller than 1%.

Table 1 shows the fractions of "light" quark, b quark and gluon jets in the three different jet classes entering the analysis of Y and Mercedes events. The classes are normal mixture jets, gluon tagged jets and b-tagged jets. "Light" quark denotes here a mixture of dus and c quarks. The jets of the normal mixture are taken from events in which the heavy hadron tag failed. Therefore they are predominantly unidentified $dusc$ quark and gluon jets. Denoting a data bin of an observable of a pure gluon, light or b quark jet sample with R_g, R_{dusc} and R_b respectively, the measured observables in the three tagged classes $R_{g_{tag}}$, $R_{b_{tag}}$ and R_{mix} can be written as:

$$\begin{aligned} R_{mix} &= p^{dusc}_{mix} \cdot R_{dusc} + p^{b}_{mix} \cdot R_b + p^{g}_{mix} \cdot R_g \\ R_{b_{tag}} &= p^{dusc}_{b_{tag}} \cdot R_{dusc} + p^{b}_{b_{tag}} \cdot R_b + p^{g}_{b_{tag}} \cdot R_g \\ R_{g_{tag}} &= p^{dusc}_{g_{tag}} \cdot R_{dusc} + p^{b}_{g_{tag}} \cdot R_b + p^{g}_{g_{tag}} \cdot R_g \end{aligned} \tag{2}$$

where the p^j_i are the fractions as e.g. shown in Table 1. The observables for the pure samples can then be obtained by solving equation 2 for R_g, R_l and R_b. The statistical

[4] There are almost always only two heavy hadrons in an event, because the $g \to q\bar{q}$ splitting into heavy quarks is strongly suppressed.

errors on the fractions p_i^j are less than 1% and are fully propagated with only a small effect on the total errors. Instead of the "light" quark sample containing *dus* and *c* quarks, a general quark sample containing *dusc* and *b* quarks can be deduced by setting $p^x_{b_{tag}} = 0$ and adding p^b_{mix} to p^{dusc}_{mix} and $p^b_{g_{tag}}$ to $p^{dusc}_{g_{tag}}$, reducing equation 2 to a 2×2 matrix equation. In a similar way the light quark sample can be reduced to only containing *dus* but no *c* quarks by hardening the heavy hadron tag and treating the *c* quarks like *b* quarks in the Monte-Carlo. This leads to the pure observables R_g, R_{dus} and R_{cb} which are related to the measured observables $R_{g_{tag}}$, $R_{b_{tag}}$ and R_{mix} in the same way as before but with different p_i^j. To correct for the limited detector acceptance, secondary reinteraction of particles and resolution of the detector, an acceptance correction factor

$$C^{acc} = \frac{R^{MC}}{R^{MC+detector}} \tag{3}$$

is also applied to the data bin by bin for each distribution. Here R^{MC} denotes pure model distributions (referring to "light" quark and gluon jets) and $R^{MC+detector}$ denotes the full simulation including detector effects treated like the data. Long lived particles like the K^0 and the Λ^0 were considered as instable when computing model distributions.

2.3 Identification of Final State Particles

For the measurement of the π^+ , K^+ and proton content in jets a combined tagging procedure based on the Cherenkov angle measurement in the RICH detector and on the ionization energy loss (dE/dx) in the TPC was applied which is described in detail in [3].

The combined application of TPC and RICH allows a continuous particle identification in the momentum range of 0.3-45.0 GeV/c. Table 2 shows which detectors were used to identify pions, kaons, and protons depending on their momentum.

<table>
<tr><th></th><th colspan="6">Momentum Range $[GeV/c]$</th></tr>
<tr><th></th><th>0.3 - 0.7</th><th>0.7 - 0.9</th><th>0.9 - 1.3</th><th>1.3 - 2.7</th><th>2.7 - 9.0</th><th>9.0 -16.0</th><th>16.0 - 45.0</th></tr>
<tr><td>π</td><td>TPC</td><td colspan="3">LRICH S</td><td colspan="3">GRICH S</td></tr>
<tr><td>K</td><td>TPC</td><td colspan="3">LRICH S</td><td>GRICH V
+
LRICH S</td><td colspan="2">GRICH S</td></tr>
<tr><td>p</td><td colspan="2">TPC</td><td>TPC
+
LRICH V</td><td>LRICH S</td><td>GRICH V
+
LRICH S</td><td>GRICH V</td><td>GRICH S</td></tr>
</table>

TPC Identification by measurement of the energy loss
LRICH S(V) Signal (Veto)-Identification with the liquid RICH
GRICH S(V) Signal (Veto)-Identification with the gas RICH

Table 2: Application ranges of the detectors for particle identification

An algorithm was developed to obtain an optimal combination of the particle identification possibilities of the TPC and the RICH. It combines the probabilities for the particle identification with the TPC and the RICH by a simple multiplication and renormalization, and predefines three different identification classes, *loose*, *standard*, and *tight*,

by using well chosen cuts on this combined probability distribution. These cuts for the particle identification probabilities allow particle identification performances with different purities R and efficiencies ε:

$$\begin{aligned} R_i^j &= \frac{\#\text{ of particles of kind } i \text{ identified as kind } j}{\#\text{ of all particles identified as kind } j}, \\ \varepsilon_i^j &= \frac{\#\text{ of particles of kind } i \text{ identified as kind } j}{\#\text{ of all particles of kind } i}. \end{aligned}$$

Figure 2 shows the efficiency of the combined particle identification of pions, kaons, and protons as a function of the momentum of the particle. The curves of the expected energy loss and the Cherenkov angle, θ_C, are shown in the upper part of Figure 2.

Figure 3 shows the resulting purities of the particle identification for Y events. To keep the influence of particle reinteractions in the detector material small, this distribution is restricted to negatively charged particles in the momentum range $p < 2.7GeV/c$ (for details see [5]). The purity matrix is predominantly diagonal (Figure 3a,f,k). The most important, however still negligible background for the pion reconstruction stems from electrons and muons. An exception are energetic electrons and muons from semileptonic hadron decays in b (and c) jets with an identification rate up to 20%. The main background for the kaon selection are pions. A kaon identification purity of $\sim 70\%$ is achieved. As the kaon production rate is almost one order of magnitude smaller than the pion production rate in hadronic Z decays, this implies a very efficient pion suppression. The lower proton identification purity in b jets is mainly due to the higher probability to identify kaons as protons because of the higher K multiplicity in b jets.

Acceptance correction of the spectra of identified particles

From the measured particle spectra I_π, I_K, and I_p of identified particles one obtains the spectra of pure hadrons S_π, S_K, and S_p by solving the equation system:

$$\begin{pmatrix} I_\pi \\ I_K \\ I_p \end{pmatrix} = \begin{pmatrix} \varepsilon_\pi^\pi & \varepsilon_K^\pi & \varepsilon_p^\pi \\ \varepsilon_\pi^K & \varepsilon_K^K & \varepsilon_p^K \\ \varepsilon_\pi^p & \varepsilon_K^p & \varepsilon_p^p \end{pmatrix} \cdot \begin{pmatrix} S_\pi \\ S_K \\ S_p \end{pmatrix} . \tag{4}$$

This correction is applied before the correction of the jet purity. The values ε_i^i denote the efficiencies that the particles i are identified correctly; the values ε_i^j with $i \neq j$ are proportional to the background of particle class j. A correction for secondary reinteraction of particles in the detector material was included in the overall correction factor Equation 3.

3 Results

For identified particles in quark and gluon jets the multiplicty and the semi-inclusive distributions as function of the momentum p, $\xi_p = \ln 1/x_p = \ln p_{jet}/p$ and the rapidity $\eta = \ln \frac{E+p_\parallel}{E-p_\parallel}$ with respect to the jet axis have been measured. For each particle also the Ratio between gluon and quark jets R and the normalized ratio $R' = R/r_{ch}$ of each of

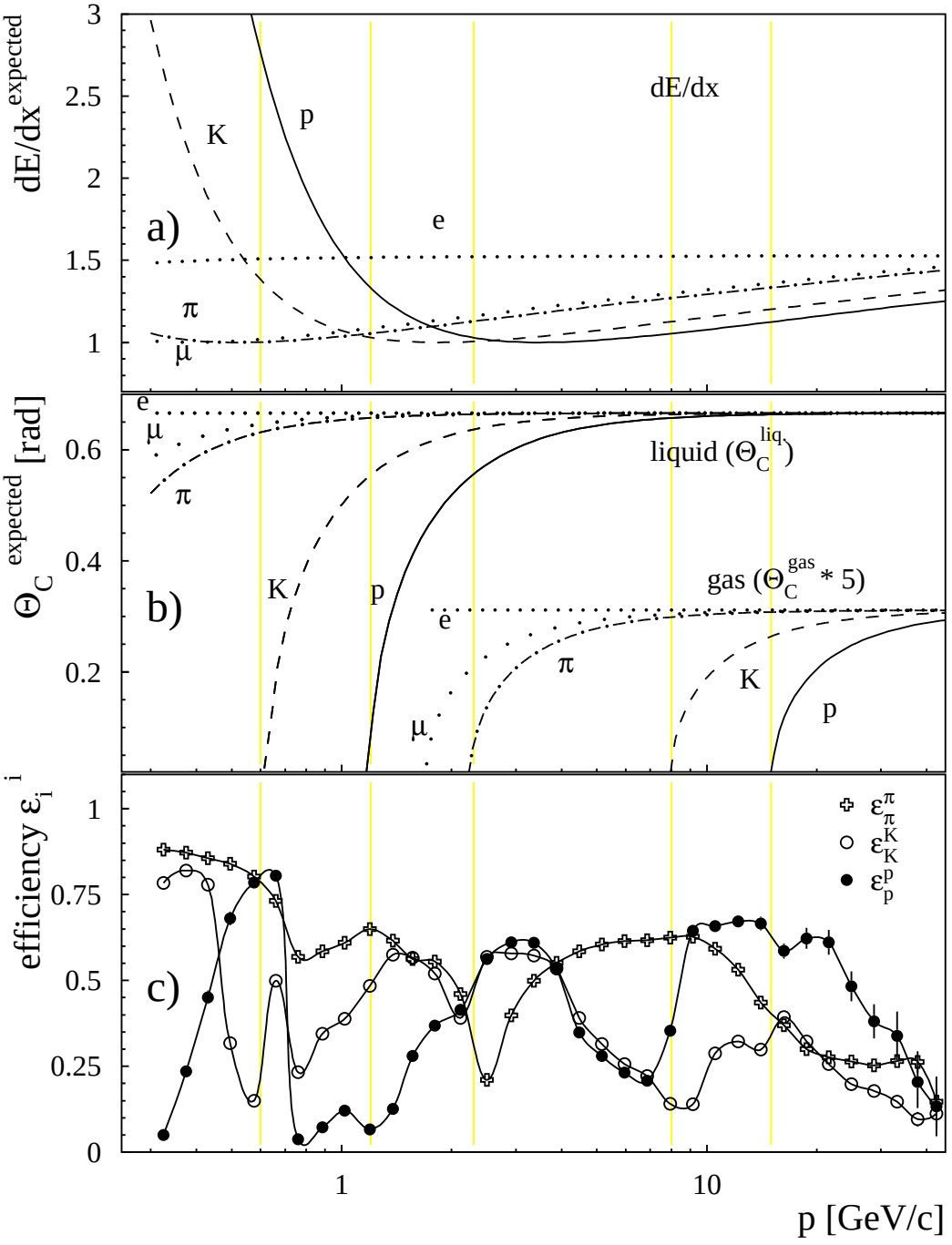

Figure 2: Curves of expected values and efficiencies of the particle identification; a) shows the curve of the expected values for specific ionization for pions (π), kaons (K), protons (p), muons (μ), and electrons (e) as a function of the momentum. b) shows the curve of the expected values for the Cherenkov angle θ_C in the liquid and gas radiator for the same particle hypotheses. ${\theta_C}^{Gas}$ was multiplied by a factor 5. The curves begin at $p = 0.3$GeV/c for the liquid radiator and at 1.7GeV/c for the gas radiator. c) shows the resulting efficiencies for Y events for the standard identification of pions, kaons and protons in the barrel of DELPHI for the 1994-95 data. Light vertical lines in all plots indicate the threshold-momenta of π, K and p identification in the two RICH radiators.

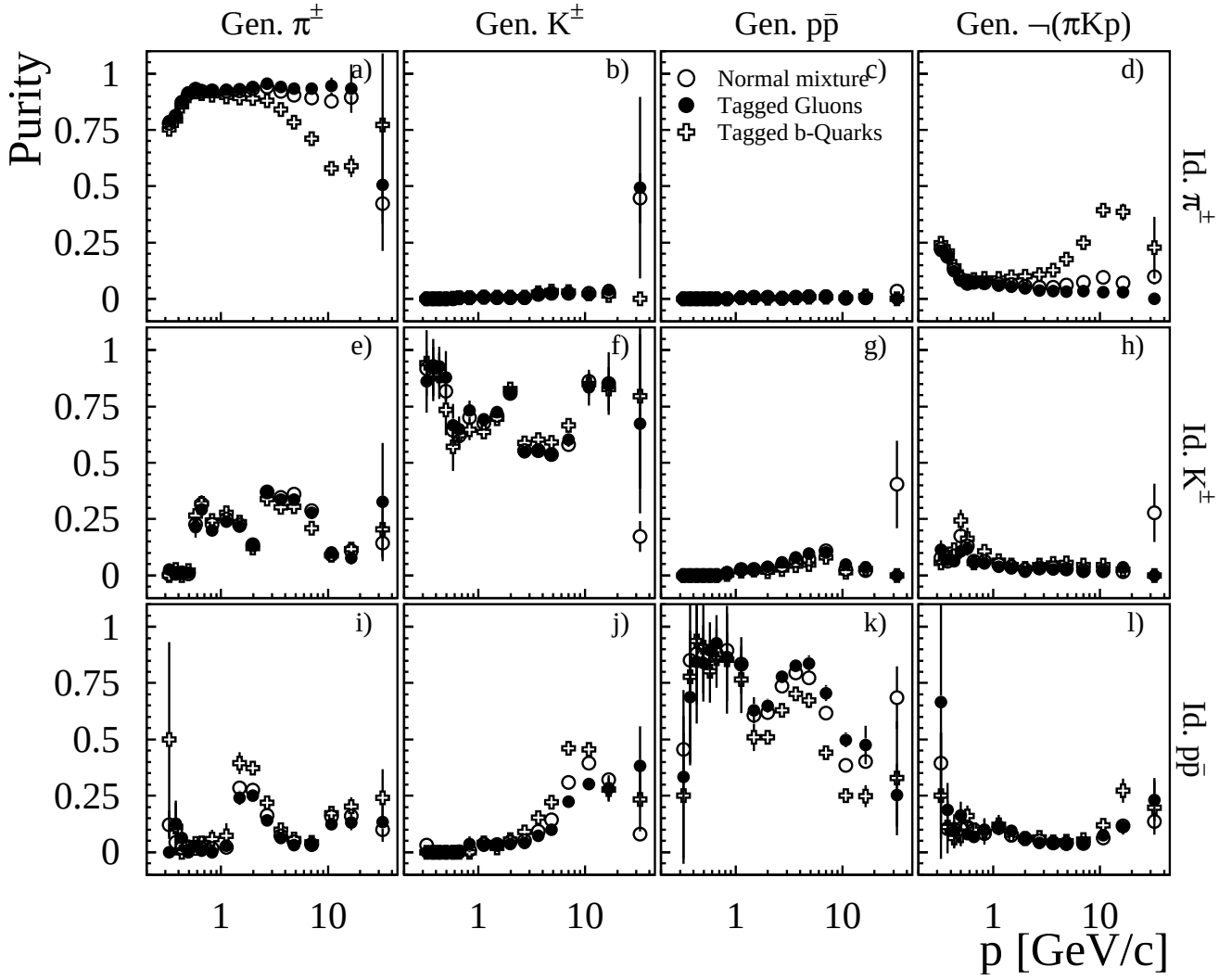

Figure 3: Purity of the particle identification in Y events. Here 'Gen.' denotes the generated flavour of the particle and 'Id.' denotes the tagged particle flavour. ¬ means not.

the observables have been studied, where r_{ch} denotes the corresponding ratio obtained for all charged particles.

Note that the particle multiplicity of jets is not a well defined subject which depends on details of the jet definition influencing the assignment of low momentum particles to the jets. The given results on multiplicities and also the particle distribution corresponding to very small momenta therefore always refer to the jet definition specified in Section 2.1.

Special emphasis here lies on the measurement of ratios in gluon to quark jets R as in these ratios the systematic error is considerably reduced as most of the systematic uncertainties cancel out. The double ratios R' stress particle specific differences between gluon and quark jets.

In this analysis gluon jets are in general compared to a "duscb" quark jet reference sample. The flavour mix of this sample is that of hadronic Z decays. For the comparison of particle multiplicities also reference samples were used where the b events ("dusc") and all heavy quark events ("dus") were removed.

3.1 Multiplicities

In Figure 4 we present the mean multiplicities N_q and N_g for identified particles in quark and gluon jets respectively, as well as their ratio, $R = N_g/N_q$, and the normalized multiplicity ratios, $R' = R/r_{ch}$.

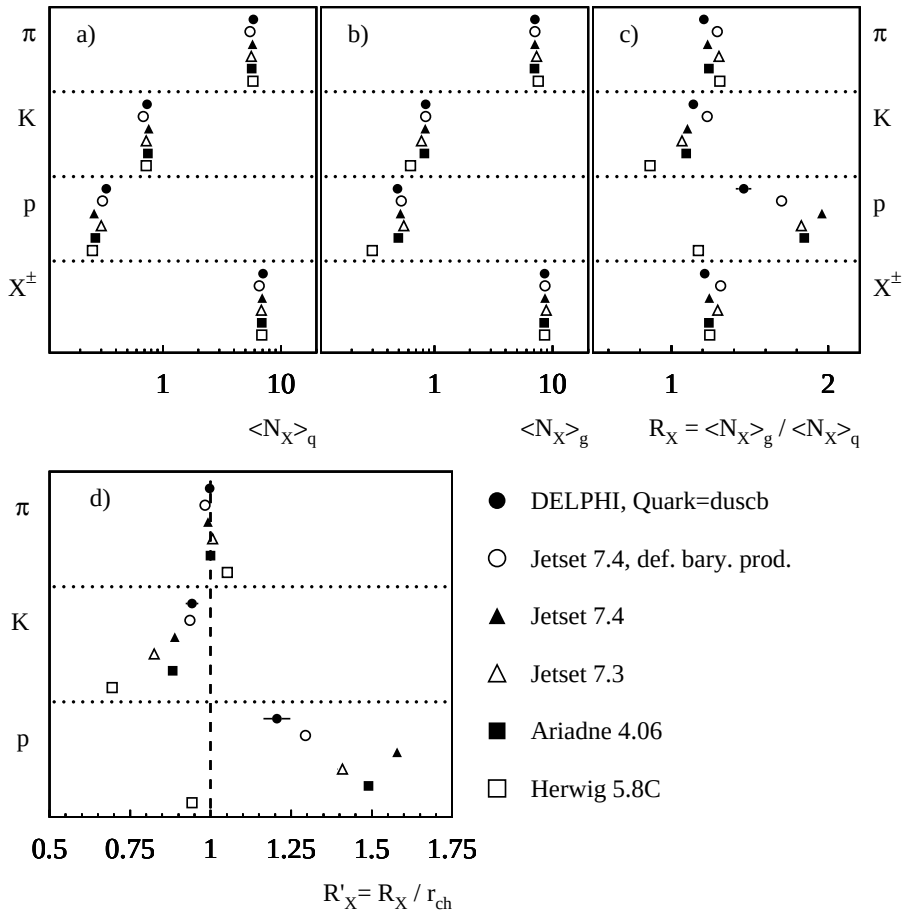

Figure 4: Mean multiplicities $N_X$and ratios of multiplicities R_X for identified particles X in quark and gluon jets of Y events compared to different Monte Carlo models.

The multiplicities measured in quark jets for identified hadrons and for all charged hadrons depend on the composition of the quark flavours within the quark jet sample. The values obtained for the multiplicities N_g and N_q and the ratios R resp. R' are given in Table 3. The determination of the systematic errors is described below. In Table 4 the normalized multiplicity ratios R' are compared to the predictions from the Monte Carlo simulations for Y and Mercedes events. The data show a significant proton enhancement in gluon jets for Y events. A similar enhancement, although less significant, is also seen in Mercedes events. The slight change observed for R'_K and R'_p (see Table 3) for different flavour compositions can be understood due to a stronger K production and a depleted proton production in events with heavy quarks.

Simulations with statistics superior to the data based on the JETSET 7.4 PS model, ARIADNE 4.08 [11], and HERWIG 5.8 [12] with parameters tuned by DELPHI [7] are compared to the data. HERWIG underestimates both the kaon and the proton production in gluon jets. In contrast JETSET and ARIADNE [5] tend to overestimate the proton production in gluon jets. The JETSET model with default baryon production [6] deviates less. The difference to the other model is that here the extra suppression at the string end, which had been introduced to describe baryon production at large scaled momenta better [7], is inactive. The excess of baryon production in gluon jets indicates that baryons are directly produced from a colour string and not via intermediate colour and baryon number neutral clusters. This is discussed in more detail in Section 3.4.

As a cross-check the summed multiplicity ratio $R_{\pi^\pm+p^\pm+K^\pm}$ was calculated. A value of 1.21 ± 0.01 was obtained in the case of Y events and 1.29 ± 0.02 in the case of Mercedes events. Both numbers are in good agreement with a direct measurement of this ratio [14] (Y: 1.235 ± 0.030, Mercedes: 1.276 ± 0.059).

For completeness Table 5 shows a comparison with measurements of other experiments. A significant excess of proton production was observed by ARGUS [13] and OPAL [14]. No quantitative comparison is, however, possible due to the different energies or event topologies.

Systematic Errors

Table 6 summarizes the influences of the most important sources of systematic error for the determination of the multiplicities and their ratios. To obtain systematic errors comparable with the statistical errors, half the difference of the value obtained when a parameter is modified from its central value is quoted as the systematic uncertainty. The single errors are added quadratically. The following sources of systematic uncertainties were examined.

1. **Decays of K^0, Λ^0**
   It was examined whether the ratios of the production rates of pions, kaons and protons in quark and gluon jets are influenced by K^0_S and Λ^0 decays. These decays are reconstructed with the program MAMMOTH [15] for the data and detector simulation. At the generated level of the simulation, these particles have been treated as stable particles.
2. **Secondary interactions**
   Another source of uncertainty stems from particles produced in reinteractions of primary particles with the detector material. Positively charged pions and protons

[5] Note that ARIADNE employs the non-perturbative hadronization model of JETSET.
[6] different from [7] $mstj(12) = 2$

Y events					
Kind	Quark	N_{Quark}	N_{Gluon}	R_X	R'_X
π	duscb	$5.852 \pm 0.036 \pm 0.071$	$7.067 \pm 0.032 \pm 0.077$	$1.208 \pm 0.009 \pm 0.020$	$0.997 \pm 0.009 \pm 0.013$
	dusc	$5.702 \pm 0.039 \pm 0.069$	$7.043 \pm 0.031 \pm 0.076$	$1.235 \pm 0.010 \pm 0.020$	$0.977 \pm 0.010 \pm 0.013$
	dus	$5.672 \pm 0.040 \pm 0.067$	$7.051 \pm 0.032 \pm 0.076$	$1.243 \pm 0.010 \pm 0.020$	$0.966 \pm 0.010 \pm 0.012$
K	duscb	$0.737 \pm 0.012 \pm 0.013$	$0.841 \pm 0.010 \pm 0.015$	$1.141 \pm 0.023 \pm 0.019$	$0.942 \pm 0.019 \pm 0.016$
	dusc	$0.692 \pm 0.013 \pm 0.013$	$0.836 \pm 0.010 \pm 0.015$	$1.208 \pm 0.026 \pm 0.020$	$0.956 \pm 0.021 \pm 0.018$
	dus	$0.637 \pm 0.013 \pm 0.012$	$0.835 \pm 0.010 \pm 0.015$	$1.310 \pm 0.031 \pm 0.022$	$1.018 \pm 0.025 \pm 0.018$
p	duscb	$0.332 \pm 0.010 \pm 0.004$	$0.485 \pm 0.009 \pm 0.008$	$1.460 \pm 0.050 \pm 0.031$	$1.205 \pm 0.041 \pm 0.025$
	dusc	$0.333 \pm 0.010 \pm 0.004$	$0.494 \pm 0.009 \pm 0.008$	$1.481 \pm 0.053 \pm 0.031$	$1.172 \pm 0.043 \pm 0.025$
	dus	$0.343 \pm 0.011 \pm 0.004$	$0.489 \pm 0.009 \pm 0.008$	$1.427 \pm 0.051 \pm 0.028$	$1.109 \pm 0.040 \pm 0.021$
$X^{\pm}$	duscb	$7.077 \pm 0.031 \pm 0.071$	$8.573 \pm 0.026 \pm 0.086$	$1.211 \pm 0.006 \pm 0.014$	1
	dusc	$6.773 \pm 0.033 \pm 0.068$	$8.560 \pm 0.026 \pm 0.086$	$1.264 \pm 0.007 \pm 0.015$	1
	dus	$6.654 \pm 0.034 \pm 0.067$	$8.559 \pm 0.026 \pm 0.086$	$1.286 \pm 0.008 \pm 0.015$	1
Mercedes events					
Kind	Quark	N_{Quark}	N_{Gluon}	R_X	R'_X
π	duscb	$6.973 \pm 0.078 \pm 0.085$	$8.962 \pm 0.133 \pm 0.096$	$1.285 \pm 0.024 \pm 0.022$	$0.998 \pm 0.023 \pm 0.012$
	dusc	$6.735 \pm 0.084 \pm 0.076$	$9.002 \pm 0.134 \pm 0.133$	$1.337 \pm 0.026 \pm 0.029$	$0.988 \pm 0.023 \pm 0.012$
	dus	$6.700 \pm 0.088 \pm 0.072$	$9.028 \pm 0.134 \pm 0.133$	$1.347 \pm 0.027 \pm 0.029$	$0.974 \pm 0.024 \pm 0.012$
K	duscb	$0.862 \pm 0.025 \pm 0.014$	$0.978 \pm 0.041 \pm 0.016$	$1.135 \pm 0.058 \pm 0.021$	$0.881 \pm 0.046 \pm 0.018$
	dusc	$0.819 \pm 0.027 \pm 0.013$	$0.982 \pm 0.042 \pm 0.011$	$1.199 \pm 0.064 \pm 0.017$	$0.886 \pm 0.049 \pm 0.016$
	dus	$0.773 \pm 0.027 \pm 0.013$	$0.981 \pm 0.042 \pm 0.011$	$1.268 \pm 0.070 \pm 0.018$	$0.917 \pm 0.052 \pm 0.017$
p	duscb	$0.401 \pm 0.022 \pm 0.006$	$0.656 \pm 0.040 \pm 0.013$	$1.635 \pm 0.134 \pm 0.049$	$1.269 \pm 0.106 \pm 0.046$
	dusc	$0.422 \pm 0.023 \pm 0.012$	$0.636 \pm 0.038 \pm 0.013$	$1.507 \pm 0.123 \pm 0.098$	$1.114 \pm 0.092 \pm 0.065$
	dus	$0.408 \pm 0.025 \pm 0.013$	$0.674 \pm 0.041 \pm 0.016$	$1.650 \pm 0.142 \pm 0.115$	$1.192 \pm 0.104 \pm 0.071$
$X^{\pm}$	duscb	$8.467 \pm 0.066 \pm 0.098$	$10.91 \pm 0.113 \pm 0.110$	$1.288 \pm 0.017 \pm 0.018$	1
	dusc	$8.085 \pm 0.071 \pm 0.097$	$10.94 \pm 0.113 \pm 0.123$	$1.353 \pm 0.018 \pm 0.025$	1
	dus	$7.942 \pm 0.074 \pm 0.089$	$10.99 \pm 0.114 \pm 0.124$	$1.384 \pm 0.019 \pm 0.024$	1

Table 3: Multiplicities and ratios of multiplicities of identified particles in quark and gluon jets .

are produced in preference. All positively charged protons were omitted in the corresponding momentum range ($p \leq 2.7$ GeV/c) to study this effect.

3. **Particle identification**
   To take uncertainties of the particle identification into account, the results for different particle identification cuts (loose, standard, and tight) were compared.
4. **Purity correction of the jets**
   The flavour composition of the normal mixture sample has been varied by imposing cuts of different strength to the event sample. In this way three samples were obtained, one with the flavour mix of Z decays, one which was depleted in b events and one depleted in b and c events. The first and second sample were used to obtain pure "duscb" and "dusc" results and the third sample to obtain "dusc" and "dus" results using the Monte Carlo.

Furthermore the results were compared to those obtained by using the CAMBRIDGE algorithm [16] instead of the DURHAM algorithm. The change of the multiplicities then is typically 2%; changes of the ratios and double ratios are much smaller. Finally a

R'_X	**Data**	**JT 74 def. bary.**	**JT 74**	**JT 73**	**AR**	**HW**
Y Events						
R'_{π^+}	$0.997 \pm 0.009 \pm 0.013$	0.98	0.99	1.01	1.00	1.05
R'_{K^+}	$0.942 \pm 0.019 \pm 0.016$	0.94	0.89	0.82	0.88	0.69
R'_p	$1.205 \pm 0.041 \pm 0.025$	1.29	1.58	1.41	1.49	0.94
Mercedes Events						
R'_{π^+}	$0.998 \pm 0.023 \pm 0.012$	1.00	1.01	1.02	1.01	1.05
R'_{K^+}	$0.881 \pm 0.046 \pm 0.018$	0.94	0.90	0.81	0.88	0.70
R'_p	$1.269 \pm 0.106 \pm 0.046$	1.20	1.43	1.38	1.37	1.11

Table 4: Normalized multiplicity ratios R'_X (for *duscb* quarks) compared to the predictions from the Monte Carlo simulations (JT 74 def. bary. = JETSET 7.4 PS with default baryon production, JT 74 = JETSET 7.4 PS, JT 73 = JETSET 7.3 PS, AR = ARIADNE 4.08, HW = HERWIG 5.8C).

Particle	This Paper Y	DELPHI [18]	OPAL three-jet [14]	ARGUS [13]
$\pi^\pm$	$0.997 \pm 0.009 \pm 0.013$	—	$1.016 \pm 0.010 \pm 0.010$	1 (def.)
$K^\pm$	$0.942 \pm 0.019 \pm 0.016$	$0.930 \pm 0.040 \pm 0.020$	$0.948 \pm 0.017 \pm 0.028$	0.86 ± 0.31
$p\bar{p}$	$1.205 \pm 0.041 \pm 0.025$	$1.120 \pm 0.110 \pm 0.040$	$1.100 \pm 0.024 \pm 0.027$	1.58 ± 0.10

Table 5: R'_X from measurements of different collaborations.

systematic error of $\lesssim 2\%$ due to track reconstruction losses as determined from the overall multiplicity measurements [17] is assumed. As both systematic errors discussed apply to particles in general, they are expected to cancel in the ratios and are therefore not included in Table 6.

All systematic errors discussed above apply to spectra of identified particles. However, the statistical uncertainty here in is general much bigger than the systematic error due to the binning of the data. Moreover many systematic uncertainties will cancel in the gluon to quark ratios which are the main subject of this paper. Systematic errors have therefore been neglected in the errors shown in the particle distributions.

3.2 Momentum Spectra

Figure 5 shows the momentum spectra of identified hadrons in quark (*duscb*) and gluon jets for Y events. The momentum spectra of kaons and protons differ significantly from those of pions. Pions are produced mainly at low momentum, both in quark and gluon jets. The likely explanation is that pions are often low energy decay products of unstable particles. The Monte Carlo generators JETSET, ARIADNE, and HERWIG describe the gross features of the measured DELPHI data. The momentum distribution of kaons in gluon jets is best described by ARIADNE. The HERWIG model shows a considerable weakness concerning the description of kaon momentum spectrum in gluon jets. The multiplicity of fast kaons is clearly underestimated. The momentum distribution

Y events										
Variable	Particle	Quarks	Value	Stat. Error [%]	Summed Error with K^0, Λ [%]	Summed Error without K^0, Λ [%]	Syst. Error [%] of K^0, Λ	Sec. Int.	Part. Id.	Purity-Corr.
N_X^q	π	duscb	5.85	0.62	-	1.21	-	1.01	0.60	0.29
		dusc	5.70	0.68	-	1.20	-	1.00	0.60	0.30
		dus	5.67	0.71	-	1.19	-	1.00	0.60	0.19
	K	duscb	0.74	1.63	-	1.77	-	0.95	1.49	0.14
		dusc	0.69	1.88	-	1.89	-	1.01	1.59	0.14
		dus	0.64	2.04	-	1.84	-	0.94	.57	0.16
	p	duscb	0.33	3.01	-	1.13	-	0.90	0.30	0.60
		dusc	0.33	3.00	-	1.12	-	0.90	0.30	0.60
		dus	0.34	3.21	-	1.09	-	0.87	.29	0.58
	$X^\pm$	duscb	7.08	0.44	-	1.01	-	1.00	0.06	0.06
		dusc	6.77	0.49	-	1.01	-	1.00	0.06	0.06
		dus	6.65	0.51	-	1.01	-	1.01	0.06	0.05
N_X^g	π	duscb	7.07	0.45	-	1.09	-	1.00	0.40	0.17
		dusc	7.04	0.44	-	1.08	-	0.99	0.38	0.17
		dus	7.05	0.45	-	1.08	-	1.01	.38	0.11
	K	duscb	0.84	1.19	-	1.75	-	0.95	1.43	0.36
		dusc	0.84	1.20	-	1.76	-	0.96	1.44	0.36
		dus	0.84	1.20	-	1.74	-	0.96	.44	0.24
	p	duscb	0.49	1.86	-	1.68	-	1.03	1.03	0.82
		dusc	0.49	1.82	-	1.64	-	1.01	1.01	0.81
		dus	0.49	1.84	-	1.57	-	1.02	.02	0.61
	$X^\pm$	duscb	8.57	0.30	-	1.01	-	1.00	0.01	0.08
		dusc	8.56	0.30	-	1.01	-	1.00	0.01	0.08
		dus	8.56	0.30	-	1.01	-	1.00	0.01	0.04
R_X	π	duscb	1.21	0.75	1.68	1.14	1.24	0.99	0.25	0.50
		dusc	1.24	0.81	1.65	1.11	1.21	0.97	0.24	0.49
		dus	1.24	0.80	1.58	1.02	1.21	0.97	.24	0.24
	K	duscb	1.14	2.02	1.65	1.63	0.26	0.96	1.31	0.09
		dusc	1.21	2.15	1.68	1.66	0.25	0.99	1.32	0.08
		dus	1.31	2.37	1.68	1.64	0.31	0.99	1.30	0.08
	p	duscb	1.46	3.42	2.13	2.11	0.27	1.03	0.96	1.58
		dusc	1.48	3.58	2.08	2.06	0.27	1.01	1.01	1.49
		dus	1.43	3.57	1.99	1.97	0.28	0.98	0.98	1.40
	$X^\pm$	duscb	1.21	0.50	1.19	0.99	0.66	0.99	0.08	0.00
		dusc	1.26	0.55	1.21	1.03	0.63	1.03	0.08	0.00
		dus	1.29	0.62	1.19	1.01	0.62	1.01	0.08	0.00
R'_X	π	duscb	1.00	0.90	1.27	1.12	0.60	1.00	0.30	0.40
		dusc	0.98	1.02	1.30	1.14	0.61	1.02	0.31	0.41
		dus	0.97	1.04	1.26	1.19	0.62	1.04	0.31	0.21
	K	duscb	0.94	2.02	1.73	1.51	0.85	0.96	1.17	0.11
		dusc	0.96	2.20	1.89	1.64	0.94	1.05	1.26	0.10
		dus	1.02	2.46	1.77	1.54	0.88	0.98	1.18	0.10
	p	duscb	1.21	3.40	2.10	2.08	0.33	1.00	0.91	1.58
		dusc	1.17	3.67	2.10	2.07	0.34	1.02	0.94	1.54
		dus	1.11	3.61	1.94	1.90	0.36	0.99	0.90	1.35

Table 6: Systematic errors for N_X^q, N_X^g, R_X and R'_X in Y events. Here X denotes the particle species π, K, p or all charged particles. The summed error displays the quadratic sum of the individual errors.

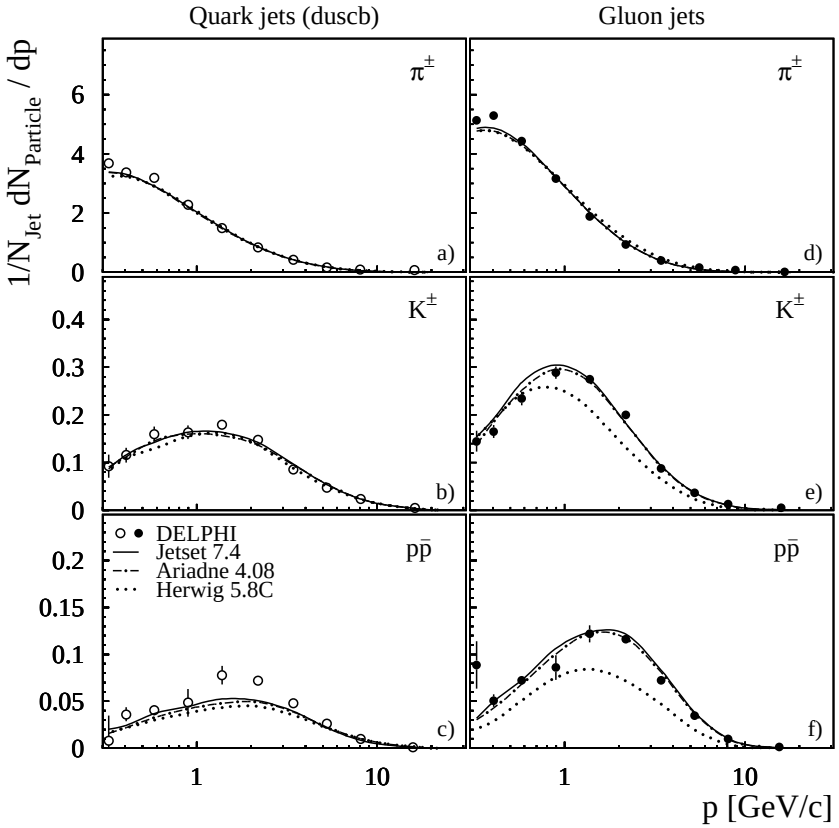

Figure 5: Momentum spectra of identified hadrons in quark and gluon jets a)-c) spectra of pions, kaons, and protons in quark jets; d)-f) corresponding spectra for gluon jets in events with Y topology. The predictions of the generator models JETSET, ARIADNE und HERWIG are drawn as lines.

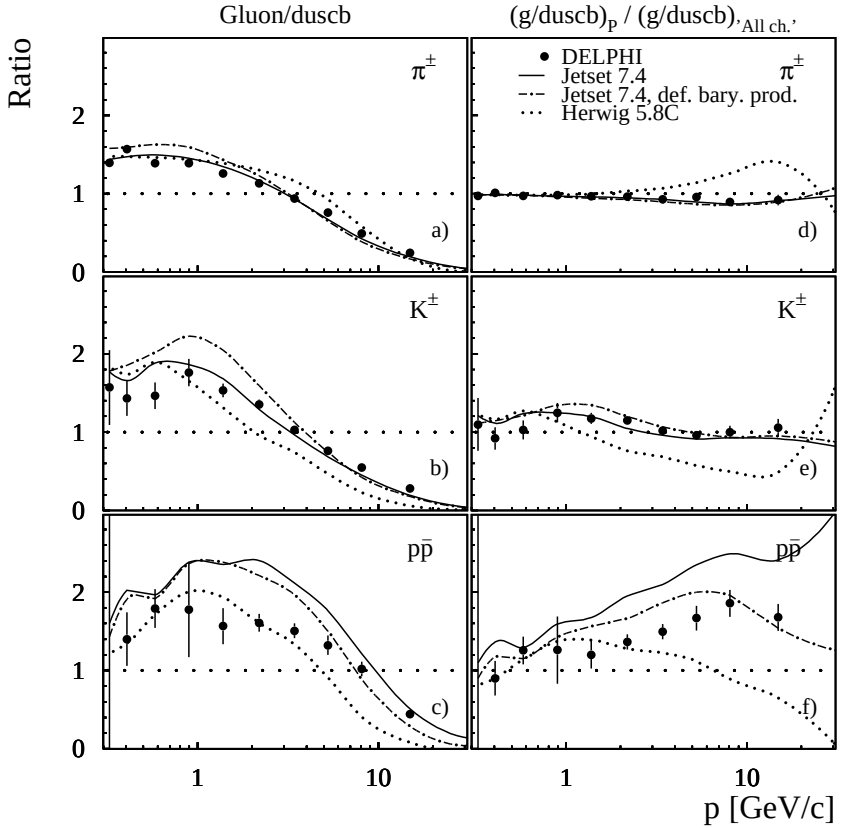

Figure 6: Ratios of the momentum spectra of identified hadrons in gluon and quark jets of Y events; a)-c) ratios of the spectra of pions, kaons, and protons in gluon jets to those in quark jets; d)-f) corresponding spectra normalized to the ratio gluon/quark for all charged particles. The predictions of the generator models JETSET, JETSET with default baryon production model and HERWIG are drawn as lines.

of protons in gluon jets is well modelled by the JETSET and ARIADNE generators but not by the HERWIG model.

Figure 6 shows the ratios of the momentum spectra of identified hadrons in gluon and quark jets . This measurement is an improvement of our previous publication [18]. More low energy particles are produced in gluon jets than in quark jets for all kinds of particles. At high particle momenta this structure is inverted. Figure 6(d,e,f) shows the corresponding ratios of the momentum spectra of Figure 6(a,b,c) normalized to the ratio of the momentum spectra of all charged particles in gluon and quark jets .

Figure 6(f) indicates that the proton enhancement in gluon jets is bigger than that for all charged particles. The overestimate of the proton production ratio by JETSET or ARIADNE (not shown) is presumably due to an extra suppression of baryon production at the end of the string (i.e. for quark jets, see also Section 3.4). A much better description is obtained using the default baryon production model without this extra suppression.

However, no direct conclusions concerning the ratios of the multiplicities can be drawn from the normalized ratios as a function of momentum, because the shapes of the momentum spectra of kaons and protons differ significantly from those of pions which dominate the all charged particle sample.

3.3 Rapidity

Figure 7 shows the rapidity spectra of identified hadrons in quark and gluon jets and Figure 8 shows the corresponding ratios. For all particles there are in the plateau, i.e. at low η, 1.6-2 times more particles in gluon jets. An excess of particles is expected due to the higher colour charge of the gluon. At high η, i.e. in the range of the leading particle only few kaons and protons are observed in gluon jets.

3.4 ξ-Spectra

Figure 9 shows the ξ_p spectra of identified hadrons in quark and gluon jets . The JETSET and ARIADNE (not shown) models provide a reasonable description over a wide range of the ξ_p spectrum. The maximum height is different for quark and gluon jets indicating different particle rates. The point of intersection of the ξ_p distributions of quark and gluon jets for pions and kaons is approximately the same, $\xi_p^{(s)} \sim 1.73$. For protons the crossing point between the quark and gluon distributions is shifted to higher momentum at $\xi_p^{(s)} \sim 0.74$. Proton production is enhanced in gluon jets, but preferentially at high momenta. This can be seen more clearly in Figure 10 which shows the normalized ratio $R_p^{'}(\xi_p)$. It is observed that this ratio is unity within errors at very small ξ_p (highest momenta) and close to unity also at large ξ_p (small momenta). A strong deviation from unity is, however, visible in the intermediate ξ_p region ($0.7 \leq \xi_p \leq 1.85$).

A surplus of baryon production in gluon jets and the observed kinematical properties can be qualitatively understood if baryons are directly produced from coloured partons or equivalently from a colour string. In a parton shower colour conservation leads to the so-called preconfinement property, that is a local compensation of colour charge in space. Alternatively the produced colour charges can always be ordered to form continuous chains or strings in space time. These strings appear naturally in the Lund fragmentation model [6] and in the progenitor model of Feynman and Field [19]. A colour string ends at the primary quarks produced in the underlying hard scattering but is spanned over the corresponding gluons. Hadron production now can be assumed to proceed via a pair-creation of a quark-anti-quark (or diquark-anti-diquark) pair and a corresponding string

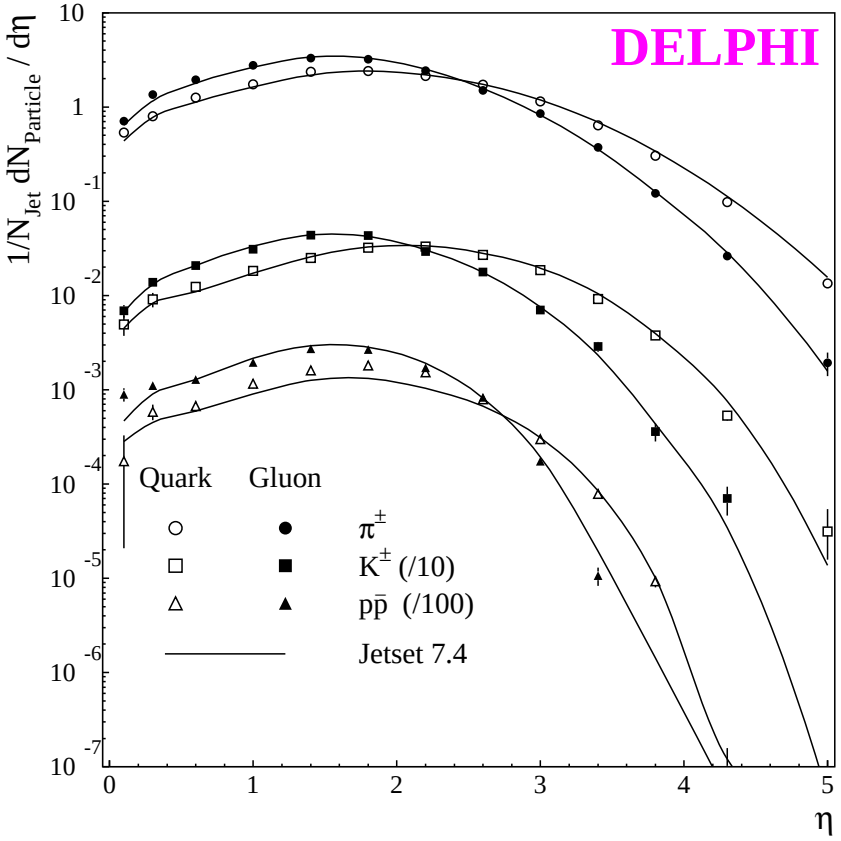

Figure 7: Rapidity spectra of identified hadrons in quark and gluon jets compared to JETSET in events with Y topology.

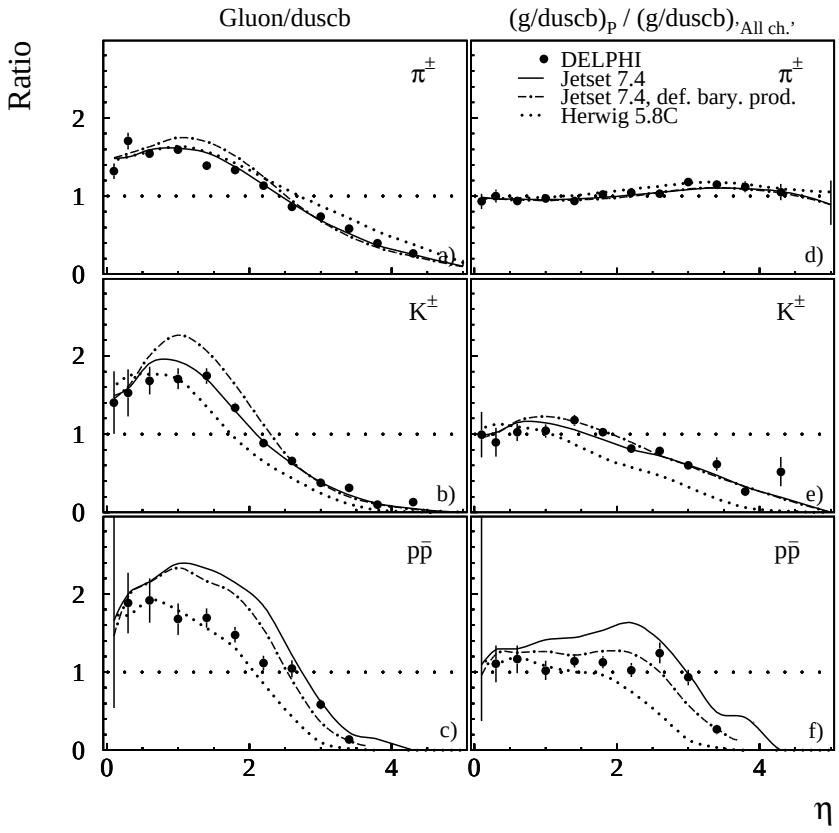

Figure 8: Ratios of the rapidity spectra of identified hadrons in gluon and quark jets from Y events; a)-c) ratios of the spectra of pions, kaons, and protons in gluon jets to those in quark jets ; d)-f) corresponding spectra normalized to the ratio gluon/quark for all charged particles; The predictions of the generator models JETSET, JETSET with the default baryon production model, and HERWIG are drawn as lines.

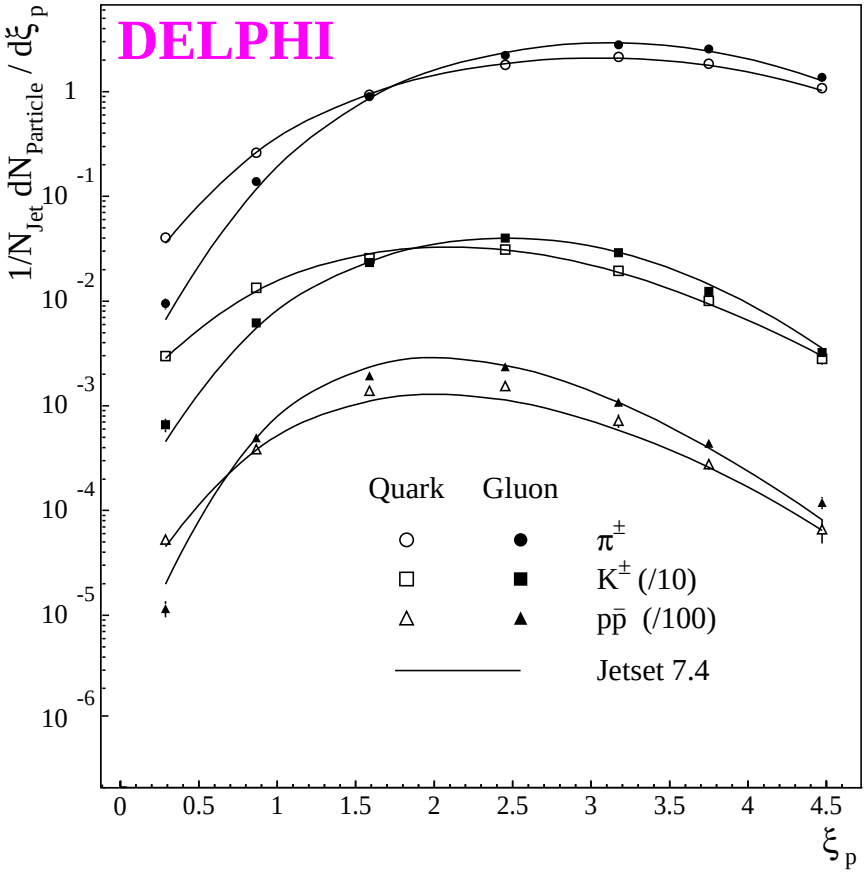

Figure 9: ξ_p spectra of identified hadrons in quark and gluon jets compared to JETSET in events with Y topology.

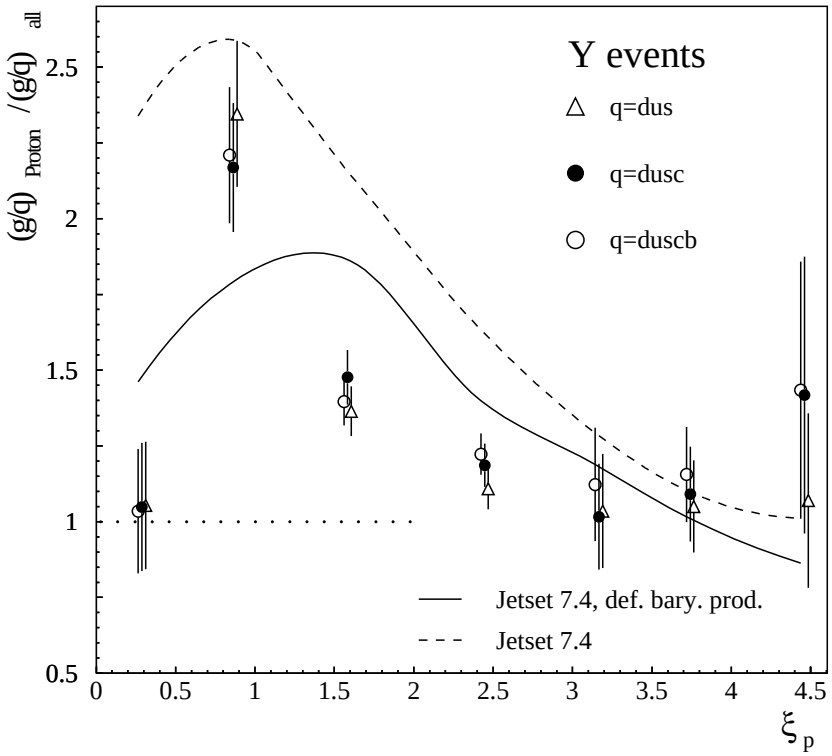

Figure 10: Normalized ratio $R'_p = R_p/r_{ch}$ for different compositions of the quark event sample (Y events).

break-up. A single break-up in the vicinity of a primary quark will produce a leading hadron, whereas close to the gluon in the centre of the string at least two breaks are needed before a hadron is formed. To produce a baryon a production of a diquark-anti-diquark pair is compelling. Now it should be noted that in the centre of a string (i.e. in the vicinity of the gluon) more possibilities exist which lead to baryon formation. A primary diquark-anti-diquark break up as well as a secondary one following a primary quark-anti-quark creation leads to baryon production (see Figure 11).

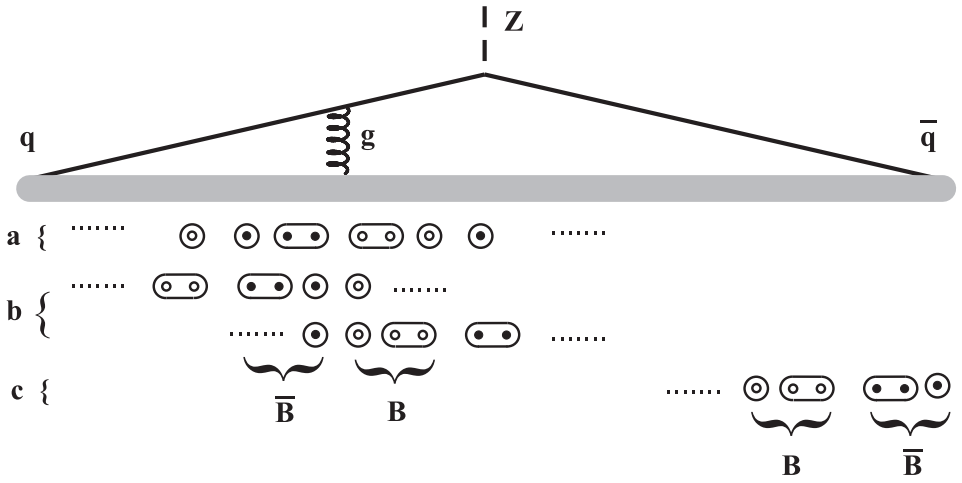

Figure 11: Different possibilities of baryon production in strings. The single points denote quarks and the double points diquarks. Open points stand for quarks and filled points for anti-quarks. Line a} illustrates a primary splitting into diquark-anti-diquark in the center of the string. Line b} shows the possibilities for secondary diquark production. Line c} shows a diquark-anti-diquark splitting at a string end.

The latter process (marked b} in Figure 11) may happen in any of the two remaining strings similarly to both original endpoints of the string (see Figure 11 c}). The first production mechanism (marked a} in Figure 11) is missing at the string end. This leads to the excess of baryons in gluon compared to quark jets. Here it is likely that two leading baryons are produced which take a large fraction of the gluon energy. Thus it is expected that the excess of baryon production centers at comparably large scaled momentum which is indeed observed (see Figure 10). At small momentum, i.e. in the momentum range where baryons from the inner part of the string between the jets are expected to contribute, the relative portion of baryon production in quark and gluon jets is approximately equal.

Although the above discussion centers around the string model it is based on quite general topological properties and is a strong indication that baryon production, and presumably also meson production, happens directly from colour objects and an intermediate step of colour and baryon number neutral objects is avoided. In particular this is also indicated by the failure of the HERWIG model to describe the surplus of proton production observed in the data.

In detail the above described mechanism will be complicated by the abundant production of resonant baryons [20]-[21] or equivalently the so-called popcorn-mechanism [6]. Further support to this interpretation comes from the observed strong energy dependence of the surplus of baryon production (compare the ARGUS measurement at $\sqrt{s} \simeq 10$GeV to this result in Table 5). The surplus of baryons in gluon jets is due to the leading

baryons. As energy and thus the multiplicity ratio in gluon to quark jets increases [1] this excess is less and less important in the double ratio $R_p^{'}$. The Lund model qualitatively describes the decrease of $R_p^{'}$ shown in Table 5.

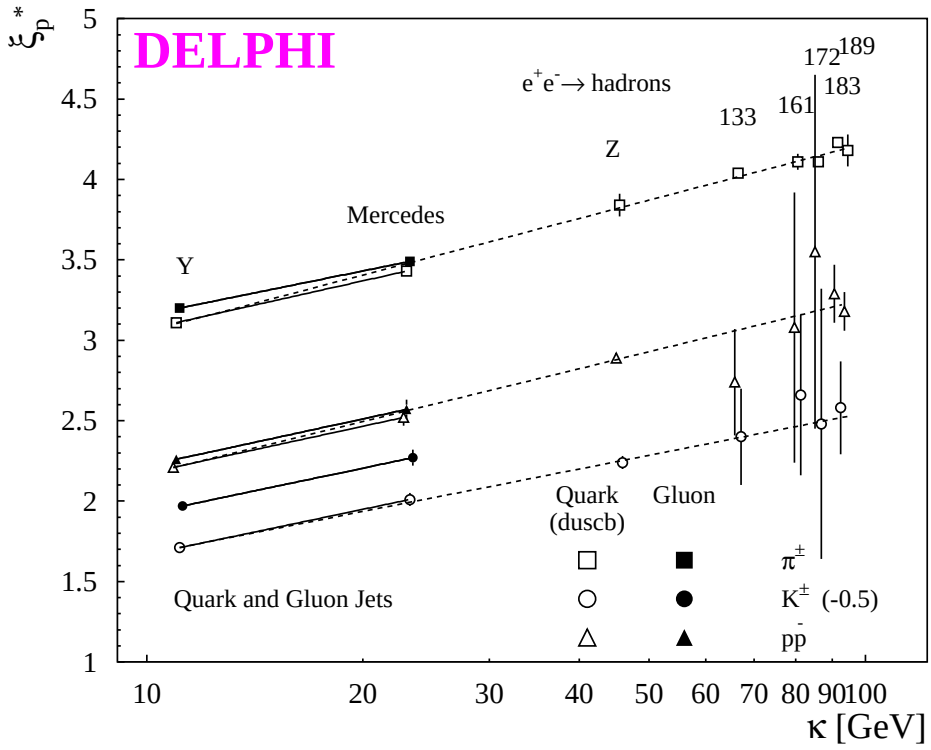

Figure 12: Fitted maxima of the ξ_p spectra. Here $\kappa = E_{jet} \sin \frac{\theta_1}{2}$ and $\kappa = E_{beam}$ denote the underlying jet scale. Observe the offset of 0.5 units for the ξ_p^* values for the $K^{\pm}$. The solid lines represent the fit to Y and Mercedes results, the dashed lines represent the fit including the e^+e^- data.

Figure 12 shows position of the maximum, ξ_p^*, of a simple Gaussian fitted to the ξ_p distributions in dependence of the scale $\kappa = E_{jet} \cdot \sin \theta_{min}/2$ with θ_{min} being the angle with respect to the closest jet, here $\theta_{min} = \theta_1$ (for a detailed discussion of jet scales see [10]). The fit results for ξ_p^* are given in Table 7. The maxima of the ξ_p distributions for protons and kaons for quark jets are shifted to smaller values (i.e. higher momenta) compared to pions as has been observed previously. It is clearly observed that the maximum is shifted to smaller ξ_p for K's in quark compared to gluon jets. To a lesser extent this is also observed for π's and p's. In MLLA/LPHD the maxima of the ξ_p spectra for gluons and quarks are expected to be almost identical [10,22]. A natural explanation for the observed difference especially for K's is the leading particle effect. In [23] it has been shown that in a scaled momentum range corresponding to the smallest ξ-bin in Figure 9 leading charged kaons (i.e. those containing a primary produced quark flavour) are about three times more often produced than non-leading kaons.

For all particles the ξ_p^* values are bigger for Mercedes than for Y events, i.e. a scale evolution of the ξ_p spectra is observed (see Figure 12 and Table 7). Assuming a general linear increase of ξ_p^* with the logarithm of the scale κ, i.e.

$$f(\xi_p^*) = a + b \ln(\kappa)$$

Y events		
par-	ξ_p^*	
ticle	quark	gluon
π	3.11 ± 0.01	3.20 ± 0.00
K	2.21 ± 0.02	2.47 ± 0.01
p	2.21 ± 0.02	2.26 ± 0.01
$X^{\pm}$	2.93 ± 0.01	3.05 ± 0.00

Mercedes events		
par-	ξ_p^*	
ticle	quark	gluon
π	3.43 ± 0.03	3.49 ± 0.02
K	2.51 ± 0.04	2.77 ± 0.05
p	2.52 ± 0.05	2.57 ± 0.06
$X^{\pm}$	3.24 ± 0.02	3.35 ± 0.02

Table 7: Maxima of the ξ_p distributions. Errors are statistical only.

the quark jet measurements extrapolate reasonably well to the measurements for overall Z events [24], and for high energy events [25]. The dashed lines in Figure 12 indicate fits including the Z and higher energy data.

It is further remarkable, that contrary to the predictions of the LPHD model, the peak values of the ξ_p distributions for kaons and protons in quark jets are almost equal (ξ_p^* values for the $K^{\pm}$ in Figure 12 are shifted by 0.5 units to avoid overlaps with the proton results.). This observation contradicts the predictions of the LPHD concept that the positions of the maxima of the ξ_p distributions are proportional to the logarithm of the mass of the corresponding particle. It has been shown already (see e.g. [26]) that mesons and baryons show a behaviour which differs from this simple expectation. This is a consequence of heavy particle decays and of the partially different masses of the decay particles in (predominantly baryon) decays. This statement is qualitatively confirmed by this analysis.

4 Summary and Conclusion

Based on a sample of about 2.2 million hadronic Z decays collected by the DELPHI detector at LEP, the production of identified particles in jets initiated by gluons or by quarks, was analysed and compared.

As observed for inclusive charged particles, the production spectrum of identified particles was found to be softer in gluon jets compared to quark jets, with a higher total multiplicity. The normalized multiplicity ratio (R') for protons in Y events was measured to be:

$$R'_p = \frac{R_p}{r_{ch}} = \frac{(N_p/N_{ch.})_g}{(N_p/N_{ch.})_q} = 1.205 \pm 0.041_{stat.} \pm 0.025_{sys.}.$$

$N_{p(ch)}$ denotes the number of protons (all charged particles). HERWIG underestimates both the kaon and the proton production in gluon jets.

This surplus of baryon production in gluon jets indicates that baryons are produced directly from coloured partons or from strings and that an intermediate state of neutral clusters (like in the HERWIG cluster model) is avoided. This interpretation is supported by the scaled energy dependence of the proton excess and by the evolution of the proton excess with energy scale.

Furthermore the ξ_p and η distributions were measured and agreement with the JETSET and ARIADNE models was found. HERWIG underestimates both the kaon and the proton production in gluon jets. The maxima of the ξ distributions of quark jets, ξ_p^*, extrapolate well with the scale κ to those obtained from all events at different centre-of-mass energies. For kaons the maximum is shifted to smaller ξ_p^* compared to gluon jets presumably because of a leading particle effect.

Acknowledgements

We thank T. Sjöstrand for useful and illuminating discussions, especially for pointing out the possible explanation of the excess of baryon production in gluon jets.
We are greatly indebted to our technical collaborators, to the members of the CERN-SL Division for the excellent performance of the LEP collider, and to the funding agencies for their support in building and operating the DELPHI detector.
We acknowledge in particular the support of
Austrian Federal Ministry of Science and Traffics, GZ 616.364/2-III/2a/98,
FNRS–FWO, Belgium,
FINEP, CNPq, CAPES, FUJB and FAPERJ, Brazil,
Czech Ministry of Industry and Trade, GA CR 202/96/0450 and GA AVCR A1010521,
Danish Natural Research Council,
Commission of the European Communities (DG XII),
Direction des Sciences de la Matière, CEA, France,
Bundesministerium für Bildung, Wissenschaft, Forschung und Technologie, Germany,
General Secretariat for Research and Technology, Greece,
National Science Foundation (NWO) and Foundation for Research on Matter (FOM), The Netherlands,
Norwegian Research Council,
State Committee for Scientific Research, Poland, 2P03B06015, 2P03B1116 and SPUB/P03/178/98,
JNICT–Junta Nacional de Investigação Científica e Tecnológica, Portugal,
Vedecka grantova agentura MS SR, Slovakia, Nr. 95/5195/134,
Ministry of Science and Technology of the Republic of Slovenia,
CICYT, Spain, AEN96–1661 and AEN96-1681,
The Swedish Natural Science Research Council,
Particle Physics and Astronomy Research Council, UK,
Department of Energy, USA, DE–FG02–94ER40817.

References

[1] DELPHI Collab., P. Abreu et al., Phys. Lett. **B449** (1999) 383.
[2] Yu.L. Dokshitzer, V.A. Khoze, A.H. Mueller, S.I. Troyan, *Basics of perturbative QCD*, Editions Frontieres, 1991.
[3] DELPHI Collab., P. Abreu et al., Nucl. Instr. Meth. **A378** (1996) 57;
DELPHI Collab,. P. Abreu et al., Nucl. Instr. Meth. **A303** (1991) 233.
[4] DELPHI Collab., P. Abreu et al., Eur. Phys. J. **C4** (1998) 1.
[5] Thesis O. Klapp, BUGh Wuppertal **WUB-DIS 99-16**;
Thesis P. Langefeld, BUGh Wuppertal **WUB-DIS 99-3**.
[6] T. Sjöstrand, Comp. Phys. Comm. **39** (1986) 346;
T. Sjöstrand, M. Bengtsson, Comp. Phys. Comm. **43** (1987) 367;
T. Sjöstrand, *JETSET 7.3 Program and Manual*, CERN-TH 6488/92.
[7] DELPHI Collab., P. Abreu et al., Z. Phys. **C73** (1996) 11.
[8] S. Catani, Yu.L. Dokshitzer, M. Olsson, G. Turnrock, B.R. Webber,
Phys. Lett. **B269** (1991) 432;
S. Bethke, Z. Kunszt, D.E. Soper, W.J. Stirling, Nuclear Physics **B370** (1992) 310.
[9] DELPHI Collab., P. Abreu et al., Z. Phys. **70** (1996) 179 (and references therein).
[10] DELPHI Collab., P. Abreu et al., Eur. Phys. J. **C13** (2000) 573.
[11] L. Loennblad, *ARIADNE 4.4 Program and Manual*, Comp. Phys. Comm. **71** (1992) 15.
[12] G. Marchesini und B.R. Webber, Nucl. Phys. **B 283** (1984) 1;
B.R. Webber, Nucl. Phys. **B 283** (1984) 492.
[13] ARGUS Collab., H. Albrecht et al. Phys. Rev. **276** (1996), 223.
[14] G. Bagliesi, *Prepared for 29th International Conference on High-Energy Physics (ICHEP 98), Vancouver, British Columbia, Canada, 23-29 Jul 1998.*
[15] DELPHI Collab., P. Abreu et al., Nucl. Instr. and Meth. **A378** (1996) 57.
[16] Yu.L. Dokshitzer, G. Leder, S. Moretti and B. Webber, JHEP**08**, (1997) 1;
S. Bentvelsen and I. Meyer, Eur. Phys. J. **C4** (1998) 623.
[17] DELPHI Collab., P. Abreu et al., Phys. Lett. **B372** (1996) 172.
[18] DELPHI Collab., P. Abreu et al., Phys. Lett. **B401** (1997) 118.
[19] R.D. Field and R.P. Feynman, Nucl. Phys. **B136** (1978), 1.
[20] OPAL Collab., G. Alexander et al., Z. Phys. **C73** (1997), 569;
DELPHI Collab., P. Abreu et al., Phys. Lett. **B475** (2000) 429.
[21] DELPHI Collab., P. Abreu et al., Phys. Lett. **B361** (1995) 207;
OPAL Collab., G. Alexander et al., Phys. Lett. **B358** (1995) 162.
[22] C.P. Fong, B.R. Webber, Phys. Lett. **B229** (1989) 289;
R.K. Ellis, W.J. Sterling, B.R. Webber, *QCD and Collider Physics*, Cambridge University Press, ISBN 0 521 58189 3 (1996).
[23] SLC Collab., K. Abe et al., *Production of charged $\pi^{\pm}, K^{\pm}$ and $p/\bar{p}$ in hadronic Z^0 decays*, hep-ex/9908033.
[24] DELPHI Collab., P. Abreu et al., Eur. Phys. J. **C 5** (1998) 585.
[25] DELPHI Collab., P. Abreu et al., *Charged and Identified Particles from the hadronic decay of W bosons and in $e^+e^- \to q\bar{q}$ from 130 to 200 GeV*, CERN-EP-2000-023, submitted to Eur. Phys. J. C.
[26] DELPHI Collab., P. Abreu et al., Nucl. Phys. **B444** (1995) 3;